

Disorder-to-order transition induced by spontaneous cooling regulation in robotic active matter

Shuaixu Hou(侯帅旭), Gao Wang(王高), Xingyu Ma(马星宇), Chuyun Wang(汪楚云), Peng Wang(王鹏), Huaicheng Chen(陈怀城), Liyu Liu(刘雳宇), and Jing Wang(王璟)

Citation: Chin. Phys. B, 2024, 33 (**7**): 078701. DOI: 10.1088/1674-1056/ad4327
Journal homepage: http://cpb.iphy.ac.cn; http://iopscience.iop.org/cpb

What follows is a list of articles you may be interested in

Identifying influential spreaders in complex networks based on density entropy and community structure

Zhan Su(苏湛), Lei Chen(陈磊), Jun Ai(艾均), Yu-Yu Zheng(郑雨语), and Na Bie(别娜)
Chin. Phys. B, 2024, 33 (**5**): 058901. DOI: 10.1088/1674-1056/ad20d6

Bio-inspired environmental adaptability of swarm active matter

Yangkai Jin(金阳凯), Gao Wang(王高), Daming Yuan(袁大明), Peilong Wang(王培龙), Jing Wang(王璟), Huaicheng Chen(陈怀城), Liyu Liu(刘雳宇), and Xingjie Zan(昝兴杰)
Chin. Phys. B, 2023, 32 (**8**): 088703. DOI: 10.1088/1674-1056/acd688

Orderly hysteresis in field-driven robot swarm active matter

Yanping Liu(刘艳萍), Gao Wang(王高), Peilong Wang(王培龙), Daming Yuan(袁大明), Shuaixu Hou(侯帅旭), Yangkai Jin(金阳凯), Jing Wang(王璟), and Liyu Liu(刘雳宇)
Chin. Phys. B, 2023, 32 (**6**): 068701. DOI: 10.1088/1674-1056/acc803

Thermal properties of a two-dimensional intrinsically curved semiflexible biopolymer

Zicong Zhou(周子聪), Yanting Wang(王延颋)
Chin. Phys. B, 2017, 26 (**3**): 038701. DOI: 10.1088/1674-1056/26/3/038701

Plasticity-induced characteristic changes of pattern dynamics and the related phase transitions in small-world neuronal networks

Huang Xu-Hui (黄旭辉), Hu Gang (胡岗)
Chin. Phys. B, 2014, 23 (**10**): 108703. DOI: 10.1088/1674-1056/23/10/108703

RAPID COMMUNICATION

Disorder-to-order transition induced by spontaneous cooling regulation in robotic active matter

Shuaixu Hou(侯帅旭)[1,†], Gao Wang(王高)[2,3,†], Xingyu Ma(马星宇)[4], Chuyun Wang(汪楚云)[5], Peng Wang(王鹏)[5], Huaicheng Chen(陈怀城)[2], Liyu Liu(刘雳宇)[1,‡], and Jing Wang(王璟)[2,§]

[1] *Chongqing Key Laboratory of Soft Condensed Matter Physics and Smart Materials, College of Physics, Chongqing University, Chongqing* 401331, *China*
[2] *Wenzhou Institute, University of Chinese Academy of Sciences, Wenzhou* 325011, *China*
[3] *School of Physical Sciences, University of Chinese Academy of Sciences, Beijing* 100049, *China*
[4] *School of Ophthalmology and Optometry, Eye Hospital, School of Biomedical Engineering, Wenzhou Medical University, Wenzhou* 325035, *China*
[5] *Postgraduate Training Base Alliance, Wenzhou Medical University, Wenzhou* 325035, *China*

(Received 1 March 2024; revised manuscript received 9 April 2024; accepted manuscript online 25 April 2024)

In classical matter systems, typical phase-transition phenomena usually stem from changes in state variables, such as temperature and pressure, induced by external regulations such as heat transfer and volume adjustment. However, in active matter systems, the self-propulsion nature of active particles endows the systems with the ability to induce unique collective-state transitions by spontaneously regulating individual properties to alter the overall states. Based on an innovative robot-swarm experimental system, we demonstrate a field-driven active matter model capable of modulating individual motion behaviors through interaction with a recoverable environmental resource field by the resource perception and consumption. In the simulated model, by gradually reducing the individual resource-conversion coefficient over time, this robotic active matter can spontaneously decrease the overall level of motion, thereby actively achieving a regulation behavior like the cooling-down control. Through simulation calculations, we discover that the spatial structures of this robotic active matter convert from disorder to order during this process, with the resulting ordered structures exhibiting a high self-adaptability on the geometry of the environmental boundaries.

Keywords: active matter, robot swarm, collective-state transitions, environmental self-adaptability

PACS: 87.15.Zg, 89.75.Fb, 05.65.+b, 87.85.St **DOI:** 10.1088/1674-1056/ad4327

1. Introduction

The phase transition is not only relevant to a variety of daily physical occurrences, but is also important in advanced scientific researches such as superconducting transition, making it a hot topic in physics. In traditional equilibrium matter systems composed of passive particles, typical phase-transition phenomena often require interactions with the external environment through physical processes such as heat transfer and mechanical work. However, in the realm of non-equilibrium active matter, which encompasses a wide array of self-propulsion particle systems[1–8] ranging from macroscopic bird flocks and fish schools to microscopic entities like cells and slime molds in nature, as well as artificially designed nanomotors and microswimmers, there is a multitude of novel collective states and transitions induced by their inherent physical mechanisms, necessitating a comprehensive research.

For active matter systems that transform external energy to drive individual motions, changes in the individual internal properties affecting the individual propulsion strength can also lead to variations in the overall motion states of the systems,[9,10] thereby triggering significant and unique collective-state transitions. For instance, in the systems composed of structurally simple active colloidal particles,[11–13] individual propulsion strength is often correlated with the rates of chemical reactions occurring on individual surfaces, hence changes of individual surface properties can induce system-wide state transitions as the reaction proceeds. Further, the motion of biological entities is regulated by more complex internal processes such as protein expression regulation and information processing. Therefore, individual internal factors such as the sensitivity to stimuli, energy conversion efficiency and decision-making strategies all play crucial roles,[14–18] closely related to collective-state transitions in important biological processes such as embryonic development, wound healing and animal migration.

On the other hand, due to the complex and dynamic direct-interactions and environment-based indirect-interactions among active matter individuals,[19–28] the microscopic quantification, analysis, and control in the rich collective phenomena of traditional active matter systems often face challenges. In recent years, the rapid development of robotic active matter has solved these problems in a sense and shown

[†]These authors contributed equally to this work.
[‡]Corresponding author. E-mail: lyliu@cqu.edu.cn
[§]Corresponding author. E-mail: wangjing@ucas.ac.cn

© 2024 Chinese Physical Society and IOP Publishing Ltd

impressive potential in deeply studying and applying fundamental principles of active matter.[29–36]

Based on an innovative robot-swarm experimental system,[37,38] we have constructed an environment-interacting field-driven active matter model. In the robotic system and corresponding simulated model, individuals sense and consume recoverable environmental resources, determining their own movements based on the principle of seeking the maximum resource intensity, thereby exhibiting a field-driven motion pattern coupled with the environmental resource field. During this process, the individual resource-conversion coefficient dictates individual speed after sensing the resource gradient. In the simulated model, by linearly decreasing the resource-conversion coefficient with time, the overall motion level of the virtual swarm gradually diminishes over time, spontaneously showing collective-behavior changes as if controlled by the effect of decreasing temperature. Simulation results indicate that during this regulation process, the order parameter ψ_6, which characterizes the degree of spatial order of the virtual robot swarm, gradually increases, demonstrating a disorder-to-order collective-state transition of the swarm. To investigate the influence of the geometry of the virtual environmental boundaries on the final spatial distribution of the virtual robot swarm, we conducted identical spontaneous-cooling-regulation simulations under different regular polygon boundaries. We found that the eventual spatial distribution states of the virtual swarm were dependent on the geometry of the environmental boundaries, showing a high environmental self-adaptability.

2. Methods

2.1. Robot–environment–interaction experimental system

In our previous work, we have built a robot–environment–interaction experimental system, which is composed of the robot swarm and the LED platform, to study the collective behaviors in active matter, and many unique physical phenomena have been observed.[37,38] In this paper, we use a simulated model to further investigate this robotic system. The main rules and key features of this robot–environment–interaction experimental system are introduced in the following content, and the corresponding simulated model is exhibited in Subsection 2.2.

As shown in Fig. 1(a), in our environment-coupled robot swarm experimental system, individual robots can sense the local light resource intensities at their current positions and affect the environment by consuming the light resources. Meanwhile, the gradually recovering environmental resource field can, in turn, influence the robots' movements through temporarily keeping the information left behind by the robots. The mutual influences between the robots and the environment endow the swarm with the field-driven collective behaviors.

Specifically, the robots move along the directions towards the maximum light resource intensity based on the local light resource gradients. In other words, the instantaneous speed of an individual robot depends on the magnitude of the local light resource gradient at its position and the robot's conversion ability on the light resource gradient, with the direction of motion consistent with the direction of the local light resource gradient, which means

$$\boldsymbol{v}_n = k_n(t)\nabla I(x_n, y_n; t), \tag{1}$$

where $\boldsymbol{v}_n$ represents the velocity of the n-th robot at time t, $k_n(t)$ represents the conversion coefficient of the robot n on the light resource gradient at time t, and ∇I represents the gradient of the local light resource at the position of the n-th robot. Similar to biochemical active matter systems, as one of the individual internal parameters, $k_n(t)$ can vary with time t. According to Eq. (1), the robots can be constrained to move within a fixed boundary by setting the initial distribution of light resource field. For instance, as shown in Fig. 1(a), the environmental resource field is set within a circular boundary as indicated by the dashed line. To provide resource gradient information at the environmental boundaries, the light resource intensities outside the boundaries are softened according to a fixed Gaussian width σ_o, which is much less than the boundary radius R_o.

On the other hand, at any given moment, an individual robot consumes environmental light resources in a two-dimensional (2D) Gaussian distribution centered at its own coordinate. The sum of all robots' consumption causes an instantaneous decrease of the intensity at the position (x, y) of the light resource field $\boldsymbol{I}$ as

$$\partial_t I(x,y) = -\sum\nolimits_n k_c \exp\left(-\frac{\left[(x-x_n)^2+(y-y_n)^2\right]}{2\sigma^2}\right), \tag{2}$$

where x_n and y_n are the position coordinates of the robot n, k_c represents the depth of the robots' resource consumption, and σ is the standard deviation of the Gaussian distribution of the consumption, which determines the spatial shape of the consumption interaction.

Combining the resource consumption with the resource search, individual robots can engage in field-driven motion as shown in Fig. 1(b). At time t_0 before the experiment, when the robot is not activated, it does not consume the local environmental resource, and its velocity is zero. At time t_1, after the robot has been activated, the local environmental resource is consumed, but the symmetric distribution of the residual resource shadow makes the robot remain stationary. At time t_2, due to the slight perturbations from the noises in the resource intensities or individual perception, the symmetric distribution of the residual resource shadow is broken, enabling the robot to detect a non-zero light resource gradient, thereby driving its movement. At time t_3, because of the positive feedback mechanism composed of the directional movement and

the resource consumption, the robot continues its movement, resulting in the field-driven motion. Significantly, the locality of the individual perception and consumption also endow the field-driven motion with the ability to partly counteract the global resource gradients, resulting in richer collective behaviors. Because the non-zero resource gradients impart the desire of the motion to the robots and the movements of the robots on the platform with high friction coefficient are completely controlled by the internal motors, once all gradients are removed, the moving robots should immediately stop at the next timestep. Thus, another key characteristic of this field-driven active matter is that they do not have the physical inertia.

After the robots go away, as shown in Fig. 1(c), consumed resource field will slowly recover with time, and the recovery rate of the environmental resource is defined as

$$\partial_t I = \frac{1}{\tau_{\mathrm{R}}}\left(I_{\mathrm{o}} - I_*\right), \tag{3}$$

where τ_{R} is the characteristic time of the resource recovery, I_{o} and I_* are the light resource intensities at the same position respectively at the initial time and the current time. Combining the resource consumption with the resource recovery, the instantaneous change of the light resource field can be calculated as

$$\begin{cases} \partial_t I = \frac{1}{\tau_{\mathrm{R}}}\left(I_{\mathrm{o}} - I_*\right) - \sum\limits_n k_{\mathrm{c}} \exp\left[-\dfrac{\left[(x-x_n)^2 + (y-y_n)^2\right]}{2\sigma^2}\right], & \text{when } I_* > 0, \\ \partial_t I = \frac{1}{\tau_{\mathrm{R}}}\left(I_{\mathrm{o}} - I_*\right), & \text{when } I_* = 0. \end{cases} \tag{4}$$

When there is more than one robot, the interaction among the robots is indirectly achieved through the environmental resource field, as shown in Fig. 1(d). When the black shadow regions left by two robots consuming environmental resources overlap, there is a mutually repulsive effect between the robots, causing them to move away from each other. Specifically, when two robots approach each other, there is a moment t_0 when the gradients of the light resource field around the robots are zero, and consequently, the robots are stationary. However, this stationary state is unstable. At time t_1, the continued superposition of the resource consumption generates the light resource gradients opposite to the previous motion directions, causing the robots to move in the opposite directions. At time t_2, as the two robots move in opposite directions, the environmental resource field experienced by the individual robot is similar to that at time t_3 in Fig. 1(b), causing the two robots to move away from each other under the influence of the field-driven effect, until the consumption ranges of the two robots no longer overlap, thus terminating their interaction. In a word, the entire robot swarm leaves delayed temporal and spatial information in the environment through the resource consumption, enabling rich interactive information exchange between the different robots and between the robots and the environment, resulting in various interesting and novel collective behaviors.

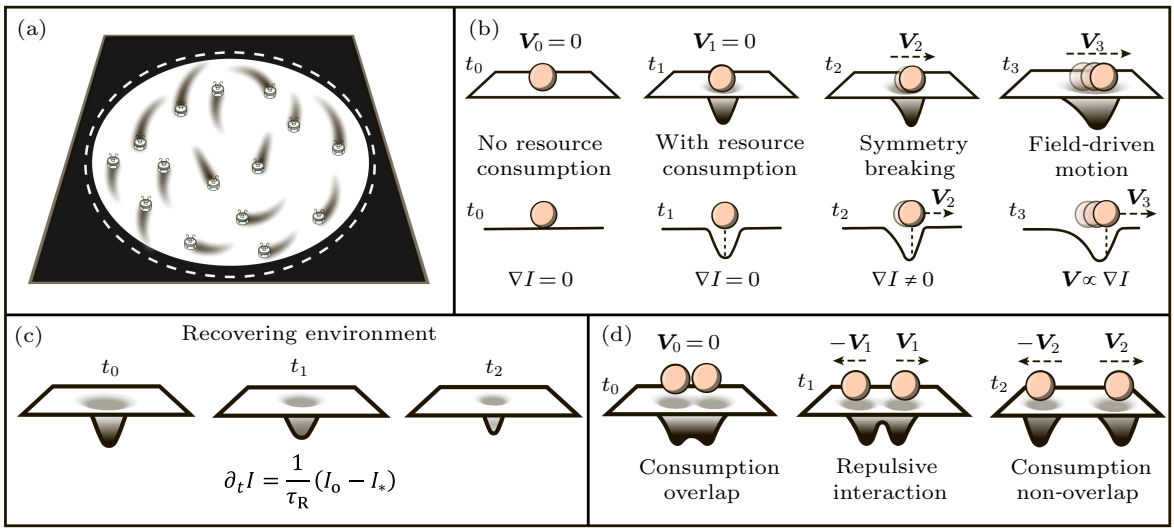


Fig. 1. Key mechanisms in the robot-swarm active-matter experimental system and the corresponding simulated model. (a) Schematic diagram for the robot-swarm active-matter experimental system. The square region represents the platform where the robot swarm is situated. The platform consists of LED lights, with a white light resource field distributed in the middle. Robots move along the directions of the resource gradients, simultaneously consuming light resources and leaving shadows at their current positions. The white dashed line marks the boundary of robotic movement. (b) The interaction process between a single robot and the environmental resource field. The robot consumes resources at its current position while moving along the direction of the light resource gradient, resulting in a field-driven motion. (c) The recovery process of environmental resource field. At time t_0, there exists a distribution of light resource field with consumption. At time t_1 and t_2, the recovery process of the environmental field is shown, where the recovery rate of the environment depends on the characteristic time τ_{R}. (d) Interactions between robots are indirectly generated through the environmental resource field. The overlapping of shadows generated by adjacent robots through the environmental resource field results in a repulsive effect between them.

2.2. Simulation model and procedures

To make further investigation on this robotic system in a more efficient way, we have constructed a simulated model to recapitulate the main collective phenomena in the experimental system. This simulated model retains all the motion rules of the real robots and adds a few new rules to the virtual robots to simulate the physical effects of the robotic entities. Each individual virtual robot is simplified as a 2D small disk in our simulated model. The initial position and orientation of each virtual robot are fully randomized at the beginning of each simulation to ensure that the results are independent of the initial spatial distribution of the virtual robots. At the start of each simulation, each virtual robot is given a random startup velocity. At any given time, an additional small positive resource gradient is applied to each virtual robot to simulate the effect of the positive feedback mechanism observed in the real robotic experiments. A symmetrical method is applied to deal with the overlapping of two virtual robots. Although there are some differences in dynamic flow, transient-state performance and quantitative details between experimental and simulated results, this simulated model has proven to be effective to study the spatial structures of the robot swarm.[38] Later in the article, all the results come from our simulation.

In all simulations, the radius of each individual virtual robot is set to 1 pixel. The truncation radius of the resource consumption for each individual virtual robot is set to 10 pixels, the consumption depth k_c is set to 15, the standard deviation σ of the Gaussian distribution of the consumption is set to 3 pixels, and the characteristic time τ_R of environmental recovery is set to 15 timesteps.

In the researches of active matter, both the strength of individual self-driven motion and environmental boundary effects play crucial roles in shaping collective behaviors. In this simulated model, the individual virtual robots can control own self-driven motion strength through regulating their conversion coefficients on the local light resource gradients. Hence, we can use the computer simulation to investigate the impact of the spontaneous regulation on the collective behaviors. For simplicity, as shown in Fig. 2(a), in this study the resource-conversion coefficient $k_n(t)$ of each virtual robot decreases linearly from 2 pixel/timestep to 0 with time, which means the maximum speed of the individual virtual robots should decrease with time, leading to a synchronized decrease in the kinetic energy of the robot swarm. In Fig. 2(a), I, II, and III respectively demonstrate the movement states of individual virtual robots under different $k_n(t)$ values. This effect is similar to the cooling process in classical physical systems, hence we term it as a spontaneous cooling regulation. In these simulations, 35 virtual robots move within a circular resource field with a radius of 25 pixels.

On the other hand, to study the influence of different environmental boundary shapes, we conducted the computer simulation to analyze and compare this regulatory effect using different shapes of regular polygon boundary conditions. In these simulations, within a regular polygonal area with an external circle radius of 40 pixels, 50 virtual robots move in the resource field.

2.3. Analysis methods

We used Voronoi tessellations[39] to preliminarily analyze the spatial distribution characteristics of the virtual robot swarm. The Voronoi tessellations divide the whole plane into different regions based on the spatial coordinates of the virtual robots, where each region contains only one virtual robot, and any position within the region is closer to the position of this virtual robot than to any positions of other virtual robots. By dividing the Voronoi cells, we can calculate the distribution of distances between the nearest-neighboring virtual robots at any given time and quantify how these distances change over time.

Furthermore, we use the hexagonal crystal parameter ψ_6 to characterize the degree of order of the spatial distribution of the virtual robot swarm. ψ_6 is a parameter describing the sixfold rotational symmetry in the arrangement of particles or atoms, commonly used to describe the order of 2D structures such as liquid crystals, crystals and glassy states.[40,41] ψ_6 is defined as

$$\psi_6 = \left\langle \frac{1}{N_j} \sum_{j'=1}^{N_j} \mathrm{e}^{\mathrm{i}6\theta_{jj'}} \right\rangle_{\mathrm{bulk}}, \tag{5}$$

where N_j is the total number of nearest neighbors to virtual robot j, $\theta_{jj'}$ is the angle between the vector connecting the virtual robot j with its nearest neighbor virtual robot j' and any fixed reference axis, and $\langle\cdot\rangle_{\mathrm{bulk}}$ denotes averaging over all virtual robots but excluding the ones at the outermost periphery of the virtual swarm.

3. Simulation results and discussion

3.1. Disorder-to-order transition induced by spontaneous cooling regulation

As the resource-conversion coefficient $k_n(t)$ decreases linearly with time in the spontaneous cooling regulation simulations in the circular resource field, the maximum and average speeds of the individual virtual robots do also decrease, as shown in Fig. 2(b). Notably, the change trends of the maximum and average speeds are not completely consistent at the initial stage, because the movements are mainly influenced by the extra random startup velocities at that stage and subsequently rely on the resource-gradient-driven motion. With the

decrease of the movement speed during the spontaneous cooling regulation, the virtual robot swarm's spatial distribution, which is represented by the cells partitioned using Voronoi tessellations, and the distribution of distances between each virtual robot and its nearest neighbors both gradually evolve, as shown in Figs. 2(c1)–2(c3) and 2(d1)–2(d3). The white disks in the Voronoi cells represent the virtual robots, and the circular boundary of the environment is outlined with the dashed lines. Figures 2(c1) and 2(d1) show the spatial and nearest-distance distribution of virtual robots at 100 timesteps, where Voronoi cells are uneven in size and shape, the distribution of environmental resource shadows is uneven, and the distribution of nearest-distances is relatively uniform, with the Gaussian fitting result being relatively flat. As shown in Figs. 2(c2) and 2(d2) at 6100 time steps, Voronoi cells gradually approach polygons and the areas of different cells tend to be consistent, while the distribution of nearest-neighbor distances gradually converges toward a specific value, as confirmed by the Gaussian fitting result. At 12190 time steps, as shown in Figs. 2(c3) and 2(d3), Voronoi cells closely resemble polygons with nearly equal areas, while the distribution of nearest-neighbor distances becomes a sharp peak. Moreover, a clear concentric layering can be observed from the center to the edge of the virtual swarm, forming a hexagonal array. In summary, the comparison of the spatial and distance distributions between the initial and final states shows that during the slow linear spontaneous cooling regulation process of the virtual robots, the areas and shapes of Voronoi cells and the distances between virtual robots gradually become consistent. On the other hand, the order parameter ψ_6 provides a more intuitive representation of the evolution of the order of the spatial distribution of the virtual swarm. As shown in Fig. 2(e), ψ_6 gradually increases with time and tends toward a specific value, indicating that the overall structure gradually approaches sixfold symmetry.

These quantitative changes in the spontaneous cooling regulation process can be explained by the following evolution process of the virtual swarm. Initially, the total kinetic energy of the virtual swarm is high, and the large instantaneous movement distances allow the individual virtual robots to traverse the potential barriers generated by two or more overlapping consumption regions. As a result, the range of the individual movement is extensive. Moreover, individual virtual robots spend relatively little time near the same positions, resulting in shallow shadows left behind, making the potential barrier effects in the resource field less pronounced. Overall, the virtual swarm demonstrates strong fluidity and appears disordered at this stage. As time progresses, the resource gradient conversion capability of virtual robots gradually declines, leading to a weakening of their movement capabilities and a reduction in their ranges of motion. On the other hand, the regions where virtual robots consume resources gradually stabilize, and repulsion barriers become stronger, restricting the movement ranges of individual virtual robots within the fixed areas generated by surrounding virtual robots' repulsive effects. Finally, the overall motion speed of the virtual swarm becomes very low, and the movement areas of individual virtual robots further shrink, making it impossible for them to traverse barriers created by other virtual robots. Since the repulsive effects come from all directions, virtual robots can only vibrate and adjust their positions near their current locations. Through continuous adjustment, these individual virtual robots are eventually distributed uniformly throughout the resource field. In conclusion, during the process of spontaneous cooling regulation in the virtual swarm, there is a significant change in the swarm's movement behavior, transitioning from a highly fluid disordered state to a more stable and uniformly distributed ordered state. This phenomenon is similar with the crystallization phenomenon in traditional matter systems during cooling.

Moreover, considering that the density and the total number of the active particles both are key parameters in traditional active matter systems, we have also done some simulations to investigate the influence of these two parameters in the spontaneous cooling regulation process. As shown in Fig. 2(f), the evolution processes of ψ_6 in the spontaneous-cooling-regulation simulations under hexagon boundaries with different radii demonstrate that when the density of the virtual robots decreases with increasing radius of the resource field, the time point of the disorder-to-order transition becomes later, and the optimal ordered structure of the virtual swarm appears at an intermediate density. This biphasic change of ψ_6 with decreasing density may come from two aspects: when the density is very high, the collision size and exhausted resource field make it difficult for the virtual robots to move to the symmetrical positions. On the contrary, when the density becomes very low, there is little interaction among the virtual robots at any time, which also makes the disorder-to-order transition take a lot of time to achieve. On the other hand, as shown in Fig. 2(g), the evolution processes of ψ_6 in the spontaneous-cooling-regulation simulations under the triangle boundaries with the same density and different total-numbers of the virtual robots demonstrate that a larger swarm makes the final spatial structure more symmetric. This result may be explained by the average effect of the large-scale swarm on the noise and defects of the swarm structure.

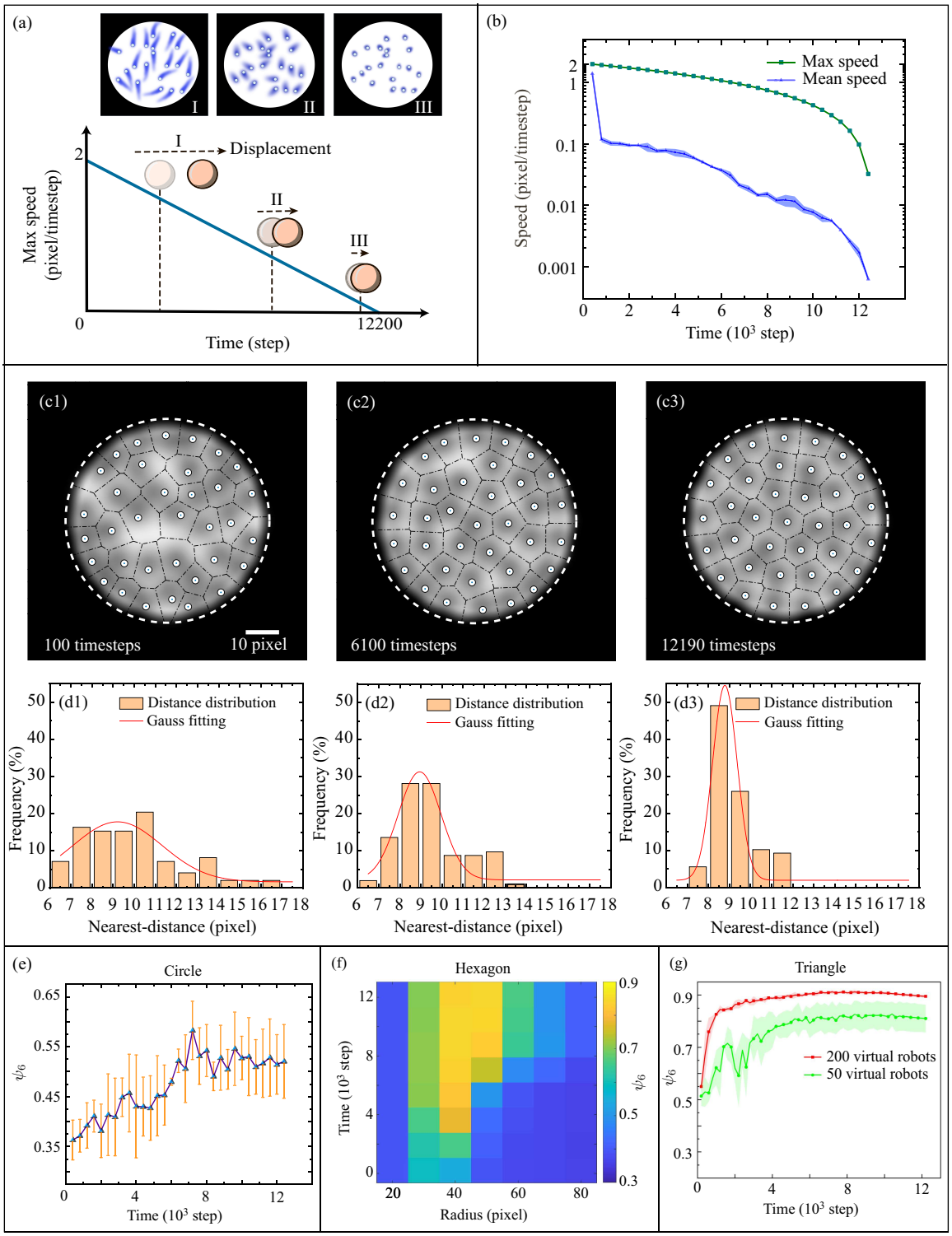


Fig. 2. Disorder-to-order collective-state transition under spontaneous cooling regulation in the simulations. (a) The impact of individual resource-conversion coefficient linearly decreasing over time on the maximum individual speed. The states of individual movement at different time are denoted as I, II, and III. (b) The variations of maximum and average speeds over time. (c)–(d) The process of the transition of spatial distribution of the virtual swarm from disorder to order over time. Panels (c1)–(c3) depict the distributions of the virtual robots within a circular boundary at 100, 6100 and 12190 timesteps, respectively. The field is divided into different cells based on the positions of the virtual robots using Voronoi tessellations. Panels (d1)–(d3) show the distributions of nearest-neighbor distances between virtual robots at corresponding times. The nearest-neighbor distance refers to the distance between a single virtual robot and the virtual robot positioned in the adjacent cell. (e) The evolution of the virtual swarm's order parameter ψ_6 over time within a circular boundary. (f) The evolutions of the order parameter ψ_6 over time in hexagon boundaries with different radii. (g) The evolutions of the order parameter ψ_6 over time in triangle boundaries with the same density and different total-numbers of the virtual robots.

3.2. Self-adaptability of spatial structure on boundary geometry

We have further investigated the influences of different geometric shapes of light resource landscape boundaries on the spontaneous cooling regulation process of the virtual swarm through the computer simulations. Figures 3(a1)–3(f1) illustrate the distributions of the initial positions of the virtual swarm within different regular-polygonal environmental

boundaries at 100 timesteps, while figures 3(a2)–3(f2) depict the distributions of the virtual robots' positions at 12190 timesteps. Obviously, the comparisons between the initial and final spatial structures show that the virtual swarms all become uniformly distributed in the spontaneous cooling regulation processes under different boundary conditions. Furthermore, the layered structures within the virtual swarms demonstrate that the influences of boundary shapes on swarms' spatial distributions propagates from the outer region to the inner. Figure 3(g) illustrates the changes in the average nearest-neighbor distances of the virtual robots over time under different boundary conditions during the spontaneous cooling regulation processes. As time progresses, all the average nearest-neighbor distances show an overall decreasing trend and eventually stabilize. Finally, the changes in ψ_6 of the virtual swarms under different boundaries are shown in Fig. 3(h), indicating an increase in the order of the spatial distribution of the swarms over time under different boundary conditions. These results indicate that the spontaneous cooling regulation processes in different shapes of regular polygonal boundaries all gradually transform the virtual swarm from initially highly mobile and disordered states to stable, uniform and ordered spatial distributions.

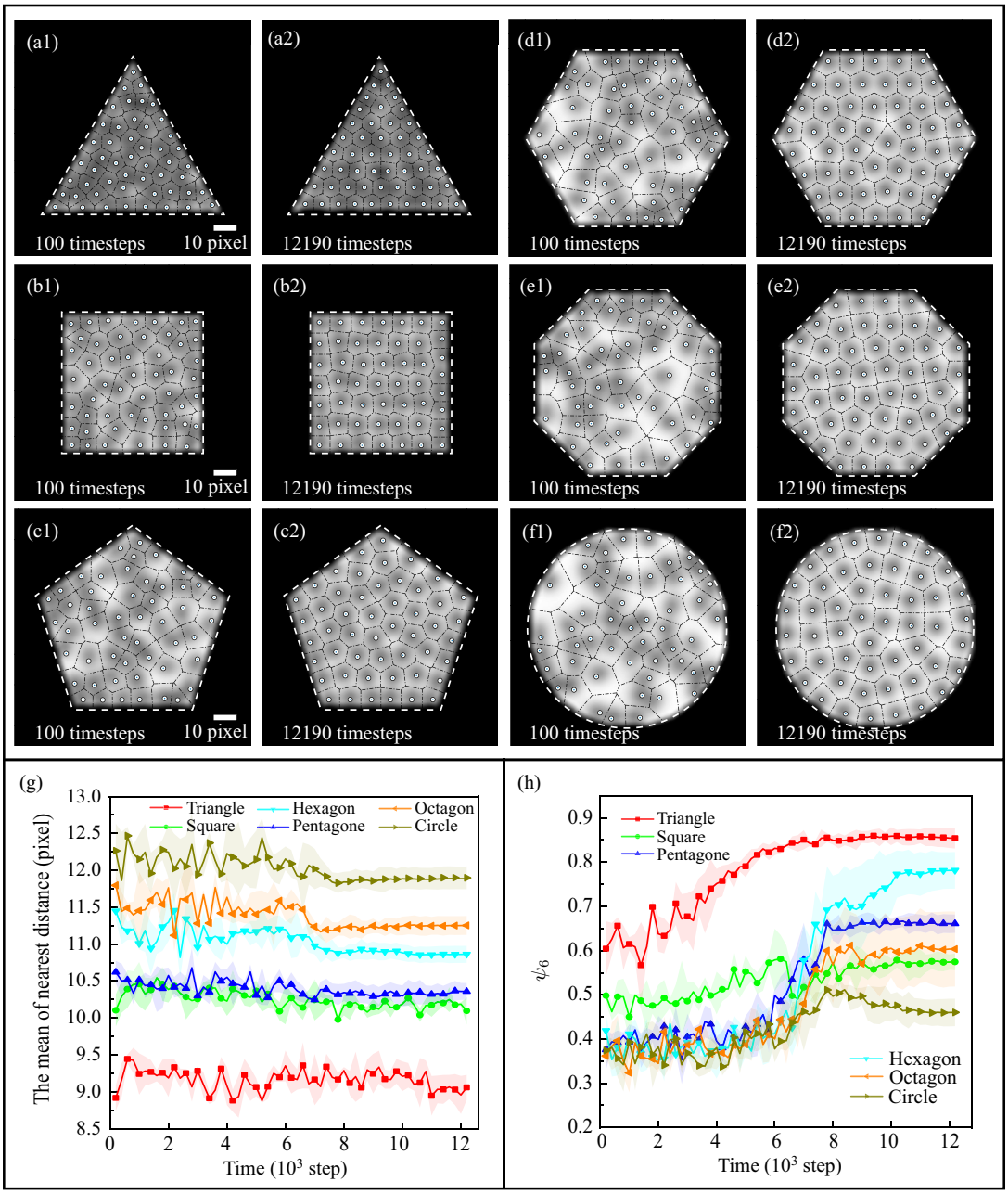


Fig. 3. Disorder-to-order transitions under spontaneous cooling regulation with different environment boundaries in simulations. (a)–(f) The changes of the spatial distributions of virtual swarms within regions of different boundary shapes of regular polygons with m edges ($m = 3, 4, 5, 6, 8, \infty$). Panels (a1)–(f1) show the distributions of virtual robots' positions at 100 timesteps, while (a2)–(f2) represent the spatial distributions at 12190 timesteps. (g) The variations of the average nearest-neighbor distances between virtual robots over time for different boundary shapes. (h) The changes in the swarms' order parameter ψ_6 over time for different boundary shapes.

The comparisons of various parameters at the final state between different boundary shapes show the differences of influences of different regular-polygon boundaries. First, according to the Voronoi cells, in the central areas of the virtual swarms under triangle and hexagon boundaries, the Voronoi cells exhibit regular patterns of interconnected hexagons, while under square boundaries, the Voronoi cells resemble squares. Second, in terms of the absolute values of the average nearest distances, under triangle boundaries, the spacing distance of the virtual swarm is the smallest, while under circular boundaries, it is the largest, as triangles have the smallest area and circles have the biggest area for a given circumscribed circle condition. Finally, the final values of ψ_6 for triangle and hexagon boundary shapes are relatively higher, while they are lower for square and circular boundary shapes. These quantitative differences are mainly caused by two factors. One is that the hexagonal lattice corresponding to the higher ψ_6 value is associated with hexagonal boundaries, whereas the square lattice corresponding to the lower ψ_6 value is associated with square boundaries. The other one is that the boundary effect is stronger under triangular boundary condition with a smaller area, and it is less impactful under circular boundary condition with a larger area, making it more challenging to influence the inner individuals. Overall, the spontaneous cooling regulation behaviors of the virtual swarm is significantly influenced by boundary effects, demonstrating a unique environmental self-adaptability. Such self-adaptability is absent in traditional crystallization processes during cooling, where lattice structures are often independent of boundary shapes.

4. Conclusion

Our simulation results demonstrate that the field-driven virtual active matter achieves a transition from disordered spatial states to ordered spatial states through spontaneous regulation of individual efficiency in converting resource gradients, akin to a temperature reduction process. This spontaneous cooling regulation behavior also exhibits strong boundary self-adaptability, whereby environmental boundary conditions can influence the final lattice type of the virtual swarm. These findings not only contribute to our understanding of important biological adaptive phenomena such as scaling of tissue formation in embryonic development,[42–44] but also provide insights for the future design of adaptive intelligent materials based on active matter.

Acknowledgements

Project supported by the National Natural Science Foundation of China (Grant No. 12174041), China Postdoctoral Science Foundation (Grant No. 2022M723118), and the Seed Grants from the Wenzhou Institute, University of Chinese Academy of Sciences (Grant No. WIUCASQD2021002).

References

[1] Zhang H P, Shi X Q and Yang M C 2022 *Physics* **51** 217 (in Chinese)
[2] Ramaswamy S 2017 *J. Stat. Mech.* **2017** 054002
[3] Needleman D and Dogic Z 2017 *Nat. Rev. Mater.* **2** 17048
[4] Cavagna A and Giardina I 2014 *Annu. Rev. Condens. Matter Phys.* **5** 183
[5] Deng J and Liu D 2021 *Bioinspir. Biomim.* **16** 046013
[6] Chen H, Zhang H, Xu T and Yu J 2021 *ACS Nano* **15** 15625
[7] Fu Y, Yu H, Zhang X, Malgaretti P, Kishore V and Wang W 2022 *Micromachines* **13** 295
[8] Servant A, Qiu F, Mazza M, Kostarelos K and Nelson B J 2015 *Adv. Mater.* **27** 2981
[9] Jiang C, Yang M, Li W, Dou S X, Wang P Y and Li H 2022 *iScience* **25** 104210
[10] Chen J X, Hu J Q and Kapral R 2024 *Adv. Sci.* **11** 2305695
[11] Wu C, Dai J, Li X, Gao L, Wang J, Liu J, Zheng J, Zhan X, Chen J, Cheng X, Yang M and Tang J 2021 *Nat. Nanotechnol.* **16** 288
[12] Hu J, Zhou S, Sun Y, Fang X and Wu L 2012 *Chem. Soc. Rev.* **41** 4356
[13] Shields C W and Velev O D 2017 *Chem.* **3** 539
[14] Fruchart M, Hanai R, Littlewood P B and Vitelli V 2021 *Nature* **592** 363
[15] Liao G J and Klapp S H L 2021 *Soft Matter* **17** 6833
[16] Kaspar C, Ravoo B J, van der Wiel W G, Wegner S V and Pernice W H P 2021 *Nature* **594** 345
[17] Roy S, Shirazi M J, Jantzen B and Abaid N 2019 *Phys. Rev. E* **100** 062415
[18] You F, Yang H X, Li Y, Du W and Wang G 2023 *Appl. Comput. Math.* **438** 127565
[19] Chen L M 2016 *Acta Phys. Sin.* **65** 186401 (in Chinese)
[20] Marchetti M C, Joanny J F, Ramaswamy S, Liverpool T B, Prost J, Rao M and Simha R A 2013 *Rev. Mod. Phys.* **85** 1143
[21] Bowick M J, Fakhri N, Marchetti M C and Ramaswamy S 2022 *Phys. Rev. X* **12** 010501
[22] Vicsek T and Zafeiris A 2012 *Phys. Rep.* **517** 71
[23] Vicsek T, Czirók A, Ben-Jacob E, Cohen I and Shochet O 1995 *Phys. Rev. Lett.* **75** 1226
[24] Liu Z T, Shi Y, Zhao Y, Chaté H, Shi X Q and Zhang T H 2021 *Proc. Natl. Acad. Sci. USA* **118** e2104724118
[25] Schockmel J, Mersch E, Vandewalle N and Lumay G 2013 *Phys. Rev. E* **87** 062201
[26] Deblais A, Barois T, Guerin T, Delville P H, Vaudaine R, Lintuvuori J S, Boudet J F, Baret J C and Kellay H 2018 *Phys. Rev. Lett.* **120** 188002
[27] Tian W D, Gu Y, Guo Y K and Chen K 2017 *Chin. Phys. B* **26** 100502
[28] Wu K T, Hishamunda J B, Chen D T N, Decamp S J, Chang Y W, Fernández-Nieves A, Fraden S and Dogic Z 2017 *Science* **355** eaal1979
[29] Yigit B, Alapan Y and Sitti M 2019 *Adv. Sci.* **6** 1801837
[30] Dorigo M, Theraulaz G and Trianni V 2021 *Proc. IEEE* **109** 1152
[31] Wu R, Zhu Y, Cai X, Wu S, Xu L and Yu T 2022 *Micromachines* **13** 1473
[32] Li S, Batra R, Brown D, Chang H D, Ranganathan N, Hoberman C, Rus D and Lipson H 2019 *Nature* **567** 361
[33] Scholz C, Engel M and Pöschel T 2018 *Nat. Commun.* **9** 931
[34] Wang G, Phan T V, Li S, Wang J, Peng Y, Chen G, Qu J, Goldman D I, Levin S A, Pienta K, Amend S, Austin R H and Liu L 2022 *Proc. Natl. Acad. Sci. USA* **119** e2120019119
[35] Jin Y, Wang G, Yuan D, Wang P, Wang J, Chen H, Liu L and Zan X 2023 *Chin. Phys. B* **32** 088703
[36] Liu P, Zhu H, Zeng Y, Du G, Ning L, Wang D, Chen K, Lu Y, Zheng N, Ye F and Yang M 2020 *Proc. Natl. Acad. Sci. USA* **117** 11901
[37] Wang G, Phan T V, Li S, Wombacher M, Qu J, Peng Y, Chen G, Goldman D I, Levin S A, Austin R H and Liu L 2021 *Phys. Rev. Lett.* **126** 108002
[38] Liu Y, Wang G, Wang P, Yuan D, Hou S, Jin Y, Wang J and Liu L 2023 *Chin. Phys. B* **32** 068701
[39] Debnath D, Gainer J S, Kilic C, Kim D, Matchev K T and Yang Y P 2016 *Eur. Phys. J. C* **76** 645
[40] Steinhardt P J, Nelson D R and Ronchetti M 1983 *Phys. Rev. B* **28** 784
[41] Eslami H, Sedaghat P and Müller-Plathe F 2018 *Phys. Chem. Chem. Phys.* **20** 27059
[42] Čapek D and Müller P 2019 *Development* **146** dev177709
[43] Wesley C C, Mishra S and Levy D L 2020 *WIREs Dev. Biol.* **9** e376
[44] Gregor T, Bialek W, van Steveninck R R D R, Tank D W and Wieschaus E F 2005 *Proc. Natl. Acad. Sci. USA* **102** 18403